Shortest-Path Percolation on Random Networks

Minsuk Kim and Filippo Radicchi*
Center for Complex Networks and Systems Research, Luddy School of Informatics, Computing, and Engineering, Indiana University, Bloomington, Indiana 47408, USA

(Received 9 February 2024; revised 28 May 2024; accepted 20 June 2024; published 26 July 2024)

We propose a bond-percolation model intended to describe the consumption, and eventual exhaustion, of resources in transport networks. Edges forming minimum-length paths connecting demanded origin-destination nodes are removed if below a certain budget. As pairs of nodes are demanded and edges are removed, the macroscopic connected component of the graph disappears, i.e., the graph undergoes a percolation transition. Here, we study such a shortest-path-percolation transition in homogeneous random graphs where pairs of demanded origin-destination nodes are randomly generated, and fully characterize it by means of finite-size scaling analysis. If budget is finite, the transition is identical to the one of ordinary percolation, where a single giant cluster shrinks as edges are removed from the graph; for infinite budget, the transition becomes more abrupt than the one of ordinary percolation, being characterized by the sudden fragmentation of the giant connected component into a multitude of clusters of similar size.

DOI: 10.1103/PhysRevLett.133.047402

Percolation theory studies the relation between the macroscopic connectedness of a system and its microscopic structure. Percolation models are fruitfully applied to many physical systems, e.g., gelation of molecules, diffusion in porous media, and forest fires [1]. In network science, percolation models are traditionally used to characterize the robustness of social, biological, and economic networks [2–8]. The existence of a macroscopic connected component in a network is interpreted as a proxy of its overall function. The connectedness of the network may be compromised by the deletion or failure of its microscopic components, either nodes (site percolation) or edges (bond percolation). The protocol used to delete the network's microscopic elements defines the specific percolation model at hand. In the ordinary percolation model, deleted microscopic elements are chosen uniformly at random [1]. Other well-known percolation models include targeted attacks [4], k-core percolation [9], cascading failures [10], continuous percolation with discontinuities [11], explosive percolation [12], fractional percolation [13], and optimal percolation [14]. These protocols can be extended to account for multiplexity [10,15] and higher-order interactions [16].

Percolation-based approaches are popular also in the analysis of dynamical processes occurring on infrastructural networks, e.g., car congestion in road networks [17–21]. By assigning a quality score to each edge (i.e., road segment) and removing edges with quality below a given threshold, the above-mentioned studies focus on how the emergence of congested clusters affects the overall function of a road network. Similar approaches are used to study road networks subject to flooding [22,23] and sidewalk networks in cities during the pandemic [24].

Here, we introduce a bond-percolation model specifically devised to mimic the utilization and progressive exhaustion of a transport network's resources. We named it as the shortest-path-percolation (SPP) model because edges are removed from the network whenever they form paths of minimum length connecting pairs of nodes. A real system that could be described by the SPP model is an airline network where travelers select minimum-cost itineraries connecting their desired origin-destination airports [25,26].

The SPP model is defined as follows. For $t > 0$, we denote with $\mathcal{G}_t = (\mathcal{V}, \mathcal{E}_t)$, composed of $N = |\mathcal{V}|$ nodes and $E_t = |\mathcal{E}_t|$ edges, the undirected and unweighted graph available to the agent t, and with $o_t \to d_t$ the origin-destination pair demanded by the agent t. If at least a path between o_t and d_t exists in $\mathcal{G}_t$, we denote with Q_t the length of the shortest one(s). The demand of the agent t can be supplied only if d_t is reachable from o_t and $Q_t \leq C$, where $C > 0$ is a tunable parameter of the model. If one shortest path satisfying this condition is identified (one path is selected at random if more than one exists), namely $(o_t = i_1, i_2, \ldots, i_{Q_t+1} = d_t)$, all edges in the path are removed from $\mathcal{G}_t$, i.e., $\mathcal{E}_t \mapsto \mathcal{E}_t \setminus \cup_{q=1}^{Q_t} (i_q, i_{q+1})$, see Fig. 1. If no path exists between o_t and d_t or if $Q_t > C$, no edge is removed from the graph. In either case, we copy the graph $\mathcal{G}_{t+1} \mapsto \mathcal{G}_t$ and then increase $t \mapsto t + 1$. The process is repeated until no more demand is requested or can be supplied.

The behavior of the SPP model depends on the structure of the graph $\mathcal{G}_1$ and the demand of the agents. Here, for simplicity, we assume that the graph $\mathcal{G}_1$ is an instance of the Erdős-Rényi (ER) model with exactly $E_1 = \bar{k}N/2$ edges, with $\bar{k}$ average degree of the graph. We further assume that

*Contact author: f.radicchi@gmail.com

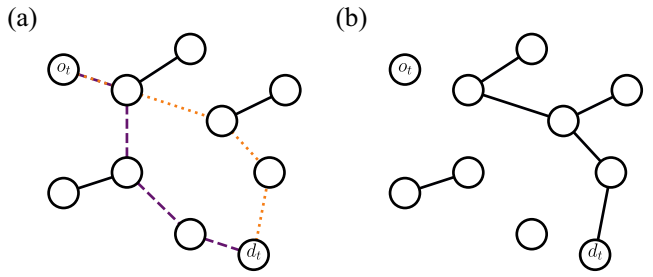

FIG. 1. The shortest-path-percolation model. (a) There are two possible shortest paths connecting the origin-destination pair $o_t \to d_t$ demanded by the agent t, denoted by orange dotted edges and purple dashed edges, respectively. The length of such shortest paths is $Q_t = 4$. (b) If the maximum length allowed in the SPP model is $C \geq 4$, one of the two shortest paths is selected at random, then all of its edges are removed from the graph. Here, all purple dashed edges are deleted, and the graph fragments into four clusters.

the origin-destination nodes $o_t \to d_t$ demanded by the agent t are chosen uniformly at random. These assumptions are not reasonable for the study of a real infrastructure and are made with the sole purpose of understanding the physics of the SPP model. They in fact allow us to contrast results obtained for the SPP model to those of other well-studied percolation models. For $C = 1$, the SPP model effectively reduces to the ordinary bond-percolation model on ER graphs displaying a smooth transition when a fraction $p_c = 1 - 1/\bar{k}$ of randomly selected edges is removed from the graph. For $1 < C \leq N$, the SPP model differentiates from the ordinary bond-percolation model as edges in the graph are no longer deleted independently, rather in a correlated fashion (note that $C = N$ is a limiting case, as the inequality $Q_t \leq C$ always holds as long as o_t and d_t are in the same connected component of the graph $\mathcal{G}_t$). We explicitly refer to the infinite-C SPP model when $\lim_{N\to\infty} C = \infty$; the finite-$C$ SPP model occurs otherwise.

We fully characterize the behavior of the SPP model on ER graphs with a systematic numerical analysis. Our results are based on a large number of independent simulations for each combination of N and C values, see Ref. [27] for details. In each realization, we first generate an ER graph with average degree $\bar{k} = 4$ and then apply the SPP model to it. For finite C, the computational complexity of the SPP model scales slightly superlinearly with the system size, so we consider networks with size up to $N = 2^{27}$. Simulating the infinite-C SPP model is subject to a higher computational burden, hence we analyze networks with size up to $N = 2^{20}$. As for the control parameters, we focus our attention to both the fraction of removed edges p as well as the raw number of demanded origin-destination pairs t. We determine the properties of the SPP transition via finite-size scaling (FSS) analysis relying on the conventional ensemble where sampled configurations correspond to independent realizations of the SPP model obtained at specific values of the control parameters [1]. All results hold when using the so-called event-based ensemble [29,30]. To construct this ensemble, we still sample one configuration from each individual realization of the SPP model; such a sampled configuration is the one corresponding to the largest change, caused by the deletion of a single edge, in the size of the largest cluster during the SPP process.

TABLE I. Critical properties of the shortest-path-percolation model. From left to right, we report: the value of the input parameter C of the SPP model, the estimate of the critical threshold p_c, the ratio of the critical exponents $\beta/\bar{\nu}$ and $\gamma/\bar{\nu}$. Estimates reported here are obtained via finite-size scaling analysis in the event-based ensemble.

C	p_c	$\beta/\bar{\nu}$	$\gamma/\bar{\nu}$
1	0.750 ± 0.001	0.32 ± 0.01	0.34 ± 0.01
2	0.701 ± 0.001	0.32 ± 0.01	0.34 ± 0.01
3	0.682 ± 0.001	0.32 ± 0.01	0.34 ± 0.01
∞	0.646 ± 0.001	0.21 ± 0.01	0.55 ± 0.01

Our main finding is that SPP belongs to the same universality class as of ordinary percolation as long as C is finite; for infinite C, the SPP transition becomes more abrupt than ordinary percolation, being characterized by a set of different critical exponents, see Table I and [27]. Results for the finite-C class are obtained by setting $C = 1$, 2, and 3 (main text and [27]); for the infinite-C class, our

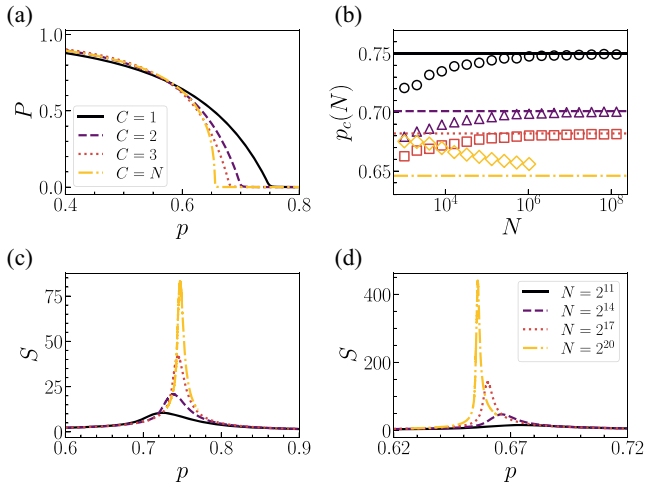

FIG. 2. Shortest-path percolation transition in the conventional ensemble. (a) Percolation strength P as a function of fraction of removed edges p with different values of C. The SPP model is applied to Erdős-Rényi (ER) graphs with size $N = 2^{20}$. (b) Pseudocritical point $p_c(N)$ as a function of N for different values of C. The horizontal line denotes the estimated critical point p_c for each C. (c) Average cluster size S as a function of p for ER graphs for different network sizes N. Here $C = 1$. (d) Similar to (c) but for $C = N$.

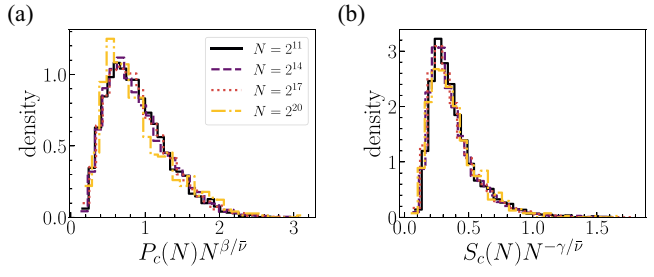

FIG. 3. Shortest-path-percolation transition in the event-based ensemble. Here we use $C = N$. (a) The distribution of $P_c(N)N^{\beta/\bar{\nu}}$ with $\beta/\bar{\nu} = 0.21$. Different curves correspond to different network sizes N. (b) Same as in (a) but for $S_c(N)N^{-\gamma/\bar{\nu}}$ with $\gamma/\bar{\nu} = 0.55$.

findings are obtained for $C = N$ (main text and [27]) as well as for $C = N^{1/3}$ and $C = \log(N)$ [27].

In Fig. 2, we report results valid under the conventional ensemble. In Fig. 2(a), we plot the percolation strength P as a function of p. We fix the network size to $N = 2^{20}$ and compare results obtained for different C values. We observe that, as C increases, the change displayed by P becomes more abrupt. The different behaviors of the finite- vs infinite-C cases are apparent by looking at how the average cluster size S changes as a function of p, see Figs. 2(c) and 2(d), with S being characterized by a peak value $S_c(N)$ occurring at the pseudocritical point $p_c(N)$. We observe that $S_c(N) \sim N^{\gamma/\bar{\nu}}$, with $\gamma/\bar{\nu} = 0.35 \pm 0.01$ if $C = 1$ and $\gamma/\bar{\nu} = 0.53 \pm 0.01$ for $C = \infty$, see Ref. [27]. Also, we find that $p_c = p_c(N) + bN^{-1/\bar{\nu}}$ for any C value, see Fig. 2(b). Not surprisingly, the value of the critical point p_c is a decreasing function of C, ranging from $p_c = 0.750 \pm 0.001$ for $C = 1$ to $p_c = 0.646 \pm 0.001$ for $C = \infty$; however, we surprisingly find that $b > 0$ and $1/\bar{\nu} \simeq 1/3$ for finite C, but $b < 0$ and $1/\bar{\nu} = 0.18 \pm 0.01$ for infinite C. The observed difference in the value of the critical exponent $\bar{\nu}$ as well as the change of the sign of the fitting parameter b denote that a fundamentally different type of percolation transition takes place depending on whether C is finite or infinite.

In Fig. 3, we display results for the FSS analysis under the event-based ensemble. Specifically, we display the collapse of the distributions of the rescaled pseudocritical observables $P_c(N)N^{\beta/\bar{\nu}}$ and $S_c(N)N^{-\gamma/\bar{\nu}}$. Both plots appearing in Fig. 3 refer to the infinite-C case; we report results valid for finite C in [27]. We find $\beta/\bar{\nu} = 0.21 \pm 0.01$ and $\gamma/\bar{\nu} = 0.55 \pm 0.01$ for $C = \infty$. Comparable values of the ratio $\beta/\bar{\nu}$ are obtained by monitoring the scaling of the peak values of the kth largest clusters, for $k = 2, 3, 4$, and 5, see Ref. [27]. Note that these estimates are compatible with the known hyperscaling relation $2\beta/\bar{\nu} + \gamma/\bar{\nu} = 1$. For finite C, we recover $\beta/\bar{\nu} \simeq \gamma/\bar{\nu} \simeq 1/\bar{\nu} \simeq 1/3$ for both the ensembles, as expected for ordinary percolation [1], see Ref. [27]. The critical exponent ratios $\beta/\bar{\nu}$ and $\gamma/\bar{\nu}$ obtained via FSS at the pseudocritical point $p_c(N)$ in the conventional ensemble are compatible with those valid for the event-based ensemble; at the critical point p_c, the estimates are different, likely because affected by finite-size effects [27].

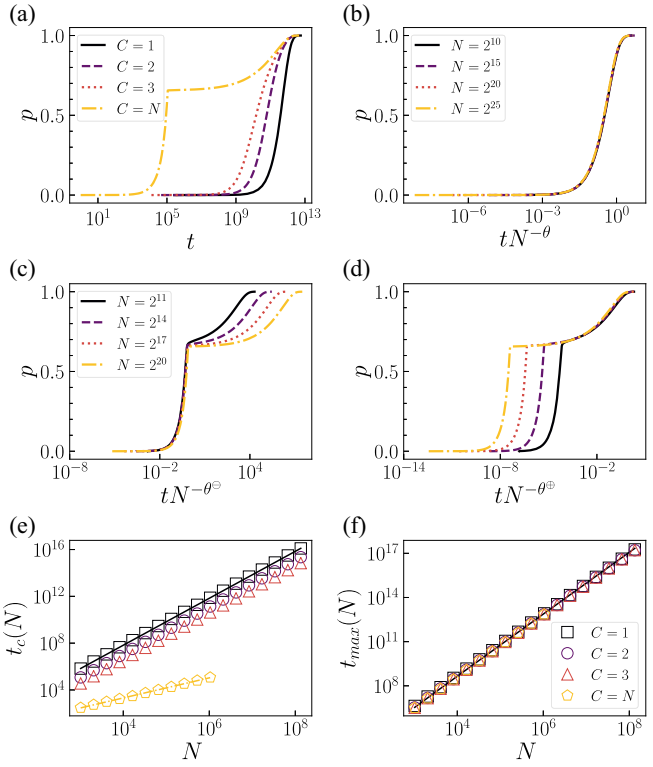

FIG. 4. Control parameters in the shortest-path percolation model. (a) The fraction of removed edges p is plotted as a function of number of demanding agents t for different values of C. Results are valid for Erdős-Rényi graphs with size $N = 2^{20}$. (b) Curve collapse for $C = 1$ and different N values. The abscissas values are rescaled as $tN^{-\theta}$, with $\theta = 2.01$, to obtain a collapse between the various curves. (c) Same as in (b), but for $C = N$. The collapse is obtained by rescaling the abscissas as $tN^{-\theta^{\ominus}}$, with $\theta^{\ominus} = 0.86$. (d) Same as in (c), but rescaling the abscissas as $tN^{-\theta^{\oplus}}$, with $\theta^{\oplus} = 2.07$. (e) Pseudocritical threshold $t_c(N)$ as a function of N for different values of C. The full black line indicates the scaling $t_c(N) \sim N^2$, whereas the dashed yellow line stands for $t_c(N) \sim N^{0.86}$. (f) Number of demanded pairs required to fully dismantle the network $t_{\max}(N)$ vs N for different values of C. The black line indicates the scaling $t_{\max}(N) \sim N^2$.

The study of the standard observables of Figs. 2 and 3 highlights a marked difference between the finite- and infinite-C transitions, however, does not convey an actual physical explanation of such a finding. A clear picture emerges from the analysis of Fig. 4, where we study the mapping between the two natural control parameters of the SPP model, i.e., p and t. For finite C, p and t are mapped one to the other by a universal smooth function that is revealed by rescaling $t \mapsto tN^{-\theta}$. We estimate $\theta = 2.01 \pm 0.01$ for $C = 1$ and similar values for other finite-C cases, see Fig. 4(e) and [27]. The scaling exponent $\theta \simeq 2$ tells us that the dismantling of the network requires to select a

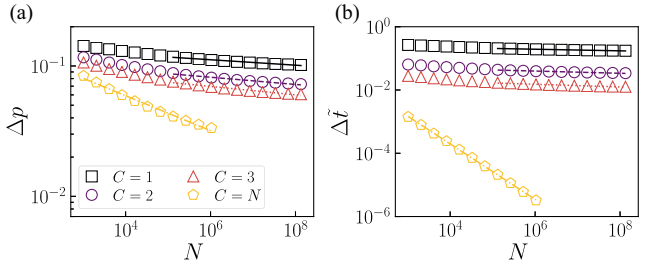

FIG. 5. Abruptness of the shortest-path-percolation transition. (a) We plot Δp vs N for different C values. Displayed lines represent the best fits of the scaling $\Delta p \sim N^{-\alpha}$. We get $\alpha = 0.02 \pm 0.01$ for $C = 1$, $\alpha = 0.03 \pm 0.01$ for $C = 2$, $\alpha = 0.03 \pm 0.01$ for $C = 3$, and $\alpha = 0.13 \pm 0.01$ for $C = N$. (b) $\Delta\tilde{t}$ vs N. Lines stand for best fits of the scaling $\Delta\tilde{t} \sim N^{-\alpha'}$. We find $\alpha' = 0.03 \pm 0.01$ for $C = 1$, $\alpha' = 0.03 \pm 0.01$ for $C = 2$, $\alpha' = 0.04 \pm 0.01$ for $C = 3$, and $\alpha' = 0.88 \pm 0.01$ for $C = N$.

number of origin-destination pairs $t_{\max}(N)$ that is proportional to the total number of node pairs in the network, see Fig. 4(f). When C is infinite, however, two distinct scaling behaviors are visible: (i) for $t \leq t_c(N)$, curve collapse is obtained by plotting p vs $tN^{-\theta^{\ominus}}$ with $\theta^{\ominus} = 0.86 \pm 0.01$, Fig. 4(e) and [27]; (ii) for $t > t_c(N)$, data collapse is obtained by rescaling $t \mapsto tN^{-\theta^{\oplus}}$ with $\theta^{\oplus} = 2.07 \pm 0.01$, Fig. 4(f) and [27]. Note that the kink point $t_c(N)$ is such that $p(t_c(N)) = p_c(N)$. The finding can be interpreted as follows. When the giant cluster is present, edges are removed with ease as a path exists between most pairs of nodes. At the beginning, the number of removed edges per pair is small as the shortest-path length between pairs of randomly selected nodes is short. However, as the graph becomes sparser, the average shortest-path length increases, so does the number of edges removed per demanded pair. Critical behavior corresponds to the consumption of a large number of edges for a small number of demanded pairs. In particular, the number of pairs that needs to be demanded to reach the critical point is a vanishing fraction of the total number of pairs of nodes in the network, as the value of the scaling exponent $\theta^{\ominus}$ indicates. After such a massive consumption of edges, the network is fragmented into multiple clusters. In this configuration, two randomly selected nodes are unlikely to belong to the same connected component. This leads to a dramatic slow down in the number of edges removed per pair of demanded origin-destination nodes. Also, individual clusters have a finite diameter, thus each of them is dismantled by an effectively finite-C SPP process, hence $\theta^{\oplus} \simeq 2$.

We assess the abruptness of the SPP transition using the same procedure as in Refs. [12,31], and measure the width of the transition window as $\Delta p = p_1 - p_2$ or $\Delta\tilde{t} = (t_1 - t_2)N^{-2}$, where p_2 and t_2 are the highest values of the control parameters for which $P > 0.5$, whereas p_1 and t_1 are the highest values of the control parameters for which $P > 1/\sqrt{N}$. The width of the transition in terms of origin-destination pairs of nodes is further normalized. As the results of Fig. 5 show, we find that $\Delta p \sim N^{-\alpha}$. The value of the scaling exponent is almost zero for finite C, e.g., $\alpha = 0.02 \pm 0.01$ for $C = 1$, denoting that the transition is continuous; for $C = N$, we find $\alpha = 0.13 \pm 0.01$, meaning that the transition is weakly discontinuous [31]. In the latter case, the exponent value is smaller than the one observed for the explosive percolation transition, thus indicating a less abrupt change of phases. The weakly discontinuous nature of the infinite-C SPP transition becomes very apparent by looking at the scaling $\Delta\tilde{t} \sim N^{-\alpha'}$, where we find $\alpha' = 0.88 \pm 0.01$. We find instead $\alpha' \simeq 0$ for finite C, e.g., $\alpha' = 0.03 \pm 0.01$ for $C = 1$, once more denoting a continuous transition.

To sum up, we introduce the shortest-path-percolation model aimed at mimicking the utilization, and eventual exhaustion, of a network's resources by agents demanding minimum-cost itineraries below a certain budget. The main finding of our systematic analysis about the application of the SPP model to Erdős-Rényi graphs is that, if budget is finite, then exhaustion occurs like in an ordinary percolation process; however, if budget is unbounded, then the network's resources are consumed abruptly, in a similar fashion as for the of explosive percolation model [12]. However, the abruptness of the SPP transition is not the result of a competitive selection criterion that takes advantage of knowledge about the cluster structure of the graph as in the explosive percolation model [31], rather caused by topological correlations among groups of deleted edges. Our findings underscore that not only dynamical processes, but also fundamental structural transitions such as percolation are radically altered by framing them in terms of path-based rather than edge-based models [32]. Also, they provide further evidence about the plausibility of range-dependent universality classes in network percolation [33–35].

The SPP model can be easily adapted to deal with arbitrary forms of demand and cost functions. Also, it can be naturally extended to directed, weighted, time-stamped graphs. All these generalizations are necessary to make the model useful for the development of computational frameworks aimed at analyzing and optimizing real-world infrastructural networks.

Acknowledgments—M. K. and F. R. thank G. Bianconi and S. Dorogovtsev for comments on the initial stages of this project. We acknowledge support by the Army Research Office under Contract No. W911NF-21-1-0194 and by the Air Force Office of Scientific Research under Award No. FA9550-21-1-0446.

The funders had no role in study design, data collection, and analysis, the decision to publish, or any opinions, findings, conclusions, or recommendations expressed in the manuscript.

[1] D. Stauffer and A. Aharony, *Introduction to Percolation Theory* (CRC Press, Boca Raton, 1985).

[2] D. S. Callaway, M. E. J. Newman, S. H. Strogatz, and D. J. Watts, Network robustness and fragility: Percolation on random graphs, Phys. Rev. Lett. **85**, 5468 (2000).

[3] R. Cohen, K. Erez, D. ben-Avraham, and S. Havlin, Resilience of the internet to random breakdowns, Phys. Rev. Lett. **85**, 4626 (2000).

[4] R. Albert, H. Jeong, and A.-L. Barabási, Error and attack tolerance of complex networks, Nature (London) **406**, 378 (2000).

[5] J. A. Dunne, R. J. Williams, and N. D. Martinez, Network structure and biodiversity loss in food webs: Robustness increases with connectance, Ecol. Lett. **5**, 558 (2002).

[6] A. G. Haldane and R. M. May, Systemic risk in banking ecosystems, Nature (London) **469**, 351 (2011).

[7] M. Li, R.-R. Liu, L. Lü, M.-B. Hu, S. Xu, and Y.-C. Zhang, Percolation on complex networks: Theory and application, Phys. Rep. **907**, 1 (2021).

[8] M. Schröder, J. Nagler, M. Timme, and D. Witthaut, Hysteretic percolation from locally optimal individual decisions, Phys. Rev. Lett. **120**, 248302 (2018).

[9] S. N. Dorogovtsev, A. V. Goltsev, and J. F. F. Mendes, K-core organization of complex networks, Phys. Rev. Lett. **96**, 040601 (2006).

[10] S. V. Buldyrev, R. Parshani, G. Paul, H. E. Stanley, and S. Havlin, Catastrophic cascade of failures in interdependent networks, Nature (London) **464**, 1025 (2010).

[11] J. Nagler, T. Tiessen, and H. W. Gutch, Continuous percolation with discontinuities, Phys. Rev. X **2**, 031009 (2012).

[12] D. Achlioptas, R. M. D'Souza, and J. Spencer, Explosive percolation in random networks, Science **323**, 1453 (2009).

[13] M. Schröder, S. E. Rahbari, and J. Nagler, Crackling noise in fractional percolation, Nat. Commun. **4**, 2222 (2013).

[14] O. Artime, M. Grassia, M. De Domenico, J. P. Gleeson, H. A. Makse, G. Mangioni, M. Perc, and F. Radicchi, Robustness and resilience of complex networks, Nat. Rev. Phys. **6**, 114 (2024).

[15] F. Radicchi, Percolation in real interdependent networks, Nat. Phys. **11**, 597 (2015).

[16] H. Sun, F. Radicchi, J. Kurths, and G. Bianconi, The dynamic nature of percolation on networks with triadic interactions, Nat. Commun. **14**, 1308 (2023).

[17] D. Li, B. Fu, Y. Wang, G. Lu, Y. Berezin, H. E. Stanley, and S. Havlin, Percolation transition in dynamical traffic network with evolving critical bottlenecks, Proc. Natl. Acad. Sci. U.S.A. **112**, 669 (2015).

[18] G. Zeng, D. Li, S. Guo, L. Gao, Z. Gao, H. E. Stanley, and S. Havlin, Switch between critical percolation modes in city traffic dynamics, Proc. Natl. Acad. Sci. U.S.A. **116**, 23 (2019).

[19] G. Zeng, J. Gao, L. Shekhtman, S. Guo, W. Lv, J. Wu, H. Liu, O. Levy, D. Li, Z. Gao *et al.*, Multiple metastable network states in urban traffic, Proc. Natl. Acad. Sci. U.S.A. **117**, 17528 (2020).

[20] M. Cogoni and G. Busonera, Stability of traffic breakup patterns in urban networks, Phys. Rev. E **104**, L012301 (2021).

[21] H. Hamedmoghadam, M. Jalili, H. L. Vu, and L. Stone, Percolation of heterogeneous flows uncovers the bottlenecks of infrastructure networks, Nat. Commun. **12**, 1254 (2021).

[22] N. Yadav, S. Chatterjee, and A. R. Ganguly, Resilience of urban transport network-of-networks under intense flood hazards exacerbated by targeted attacks, Sci. Rep. **10**, 10350 (2020).

[23] S. Dong, X. Gao, A. Mostafavi, and J. Gao, Modest flooding can trigger catastrophic road network collapse due to compound failure, Commun. Earth Environ. **3**, 38 (2022).

[24] D. Rhoads, A. Solé-Ribalta, M. C. González, and J. Borge-Holthoefer, A sustainable strategy for open streets in (post) pandemic cities, Commun. Phys. **4**, 183 (2021).

[25] M. Zanin and F. Lillo, Modelling the air transport with complex networks: A short review, Eur. Phys. J. Special Topics **215**, 5 (2013).

[26] T. Verma, F. Russmann, N. A. Araújo, J. Nagler, and H. J. Herrmann, Emergence of core–peripheries in networks, Nat. Commun. **7**, 10441 (2016).

[27] See Supplemental Material at http://link.aps.org/supplemental/10.1103/PhysRevLett.133.047402, which includes Ref. [28], for details on the implementation of the model and for extensive results of the finite-size scaling analysis.

[28] M. E. J. Newman and R. M. Ziff, Efficient Monte Carlo algorithm and high-precision results for percolation, Phys. Rev. Lett. **85**, 4104 (2000).

[29] J. Fan, J. Meng, Y. Liu, A. A. Saberi, J. Kurths, and J. Nagler, Universal gap scaling in percolation, Nat. Phys. **16**, 455 (2020).

[30] M. Li, J. Wang, and Y. Deng, Explosive percolation obeys standard finite-size scaling in an event-based ensemble, Phys. Rev. Lett. **130**, 147101 (2023).

[31] J. Nagler, A. Levina, and M. Timme, Impact of single links in competitive percolation, Nat. Phys. **7**, 265 (2011).

[32] R. Lambiotte, M. Rosvall, and I. Scholtes, From networks to optimal higher-order models of complex systems, Nat. Phys. **15**, 313 (2019).

[33] N. Almeira, O. V. Billoni, and J. I. Perotti, Scaling of percolation transitions on Erdös-Rényi networks under centrality-based attacks, Phys. Rev. E **101**, 012306 (2020).

[34] N. Almeira, J. I. Perotti, A. Chacoma, and O. V. Billoni, Explosive dismantling of two-dimensional random lattices under betweenness centrality attacks, Chaos, Solitons Fractals **153**, 111529 (2021).

[35] L. Cirigliano, C. Castellano, and G. Timár, Extended-range percolation in complex networks, Phys. Rev. E **108**, 044304 (2023).